Cosmic-Ray Ionization Rate in Protoplanetary Disks with Sheared Magnetic Fields

AUTHOR(S):

Fujii, Yuri I.; Kimura, Shigeo S.

The Astrophysical Journal Letters, 937:L37 (9pp), 2022 October 1 https://doi.org/10.3847/2041-8213/ac86c2

Cosmic-Ray Ionization Rate in Protoplanetary Disks with Sheared Magnetic Fields

Yuri I. Fujii[1,2] and Shigeo S. Kimura[3,4]
[1] Graduate School of Human and Environmental Studies, Kyoto University, Yoshida-Nihonmatsu, Sakyo, Kyoto 606-8501, Japan; fujii@gaia.h.kyoto-u.ac.jp
[2] Department of Physics, Nagoya University, Furo-cho, Chikusa-ku, Nagoya, Aichi 464-8602, Japan
[3] Frontier Research Institute for Interdisciplinary Sciences, Tohoku University, Sendai 980-8578, Japan
[4] Astronomical Institute, Graduate School of Science, Tohoku University, Sendai 980-8578, Japan
Received 2022 May 6; revised 2022 August 3; accepted 2022 August 3; published 2022 September 30

Abstract

We investigate the effects of magnetic-field configurations on the ionization rate by cosmic rays in protoplanetary disks. First, we consider cosmic-ray propagation from the interstellar medium (ISM) to the protoplanetary disks and showed that the cosmic-ray density around the disk should be 2 times lower than the ISM value. Then, we compute the attenuation of cosmic rays in protoplanetary disks. The magnetic fields in the disk are stretched to the azimuthal directions, and cosmic rays need to detour while propagating to the midplane. Our results show that the detouring effectively enhances the column density by about two orders of magnitude. We employ a typical ionization rate by cosmic rays in diffuse ISM, which is considered too high to be consistent with observations of protoplanetary disks, and find that the cosmic rays are significantly shielded at the midplane. In the case of the disk around IM Lup, the midplane ionization rate is very low for $r \lesssim 100$ au, while the value is as large as a diffuse ISM in the outer radii. Our results are consistent with the recent Atacama Large Millimeter/submillimeter Array observation that indicates the radial gradient in the cosmic-ray ionization rate. The high ionization rate in the outer radii of disks may activate the magnetorotational instability that was thought to be suppressed due to ambipolar diffusion. These results will have a strong influence on the dynamical and chemical evolutions of protoplanetary disks.

Key words: Ionization – Protoplanetary disks – Cosmic rays – Magnetic fields

1. Introduction

Protoplanetary disks are the birthplaces of planets. They consist of weakly ionized gas, and their dynamics are mainly governed by the magnetohydrodynamic (MHD) processes. Hence, the ionization degree inside the disks determines the fate of the protoplanetary disks (e.g., Sano et al. 2000; Wardle 2007; Gressel et al. 2012, 2015; Bai 2017; Béthune et al. 2017; Mori et al. 2019). Ionization also affects the chemical reactions in the disk, which is crucial to interpreting the observational data of Atacama Large Millimeter/submillimeter Array (ALMA; e.g., Walsh et al. 2012; Eistrup et al. 2016; Aikawa et al. 2021; Law et al. 2021; Notsu et al. 2021; Öberg et al. 2021).

Cosmic rays are an essential ionization source in protoplanetary disks. Protostellar radiations, including ultraviolet and X-rays, are the most powerful ionization source in the upper layer of the disk. However, they are easily blocked by the disk gas, and their ionization rates at the midplane are strongly suppressed (Igea & Glassgold 1999; Ercolano & Glassgold 2013). Cosmic rays have a stronger penetration power, and thus, they are expected to be the dominant source of ionization at the midplane of the inner disk (e.g., Gammie 1996; Sano et al. 2000; Wardle 2007; Okuzumi 2009; Fujii et al. 2011), although many previous studies on the ionization degree of protoplanetary disks only consider X-ray ionization (e.g., Glassgold et al. 1997; Fromang et al. 2002; Ilgner & Nelson 2006; Turner & Sano 2008). In the deepest part of the disk, where even cosmic rays cannot penetrate, the ionization floor is determined by radionuclides. The ionization rate by cosmic rays in protoplanetary disks is still controversial due to the uncertainty of cosmic-ray intensity there. Cleeves et al. (2013, 2014, 2015) discussed the modulation of cosmic rays by stellar winds from T-Tauri stars, i.e., T-Tauriosphere. Cosmic rays can be produced by protostellar activities, which are known as stellar energetic particles. These may also be an important ionization source, especially in the surface layer of the disk (Turner & Drake 2009; Padovani et al. 2015, 2016; Rab et al. 2017; Fraschetti et al. 2018).

Most of the previous studies assumed that the energy density of cosmic rays at the surface of a protoplanetary disk is the same as that in an interstellar medium (ISM; e.g., Gammie 1996; Sano et al. 2000; Furuya et al. 2013). They also consider that cosmic rays travel to the disk midplane in the shortest path, i.e., cosmic rays enter the protoplanetary disk straightly from the vertical direction. In reality, the shear motion in protoplanetary disks stretches the magnetic field, and cosmic rays travel only along the magnetic-field lines due to their small gyration radii (see Figure 1). Thus, the cosmic rays should detour to reach into the protoplanetary disks, which changes both the cosmic-ray energy density and the penetration depth. Padovani et al. (2018) estimated the cosmic-ray ionization rate in the inner radii of a protoplanetary disk with taking the effect of the disk magnetic field into account. In this Letter, we consider the magnetic fields that are connected to the molecular cloud and discuss the effects of sheared field lines on the cosmic-ray ionization rate in global protoplanetary disks.

2. Focusing and Reflecting Cosmic-Ray Particles

We consider the magnetic-field configuration shown in Figure 1, where magnetic fields threading the protoplanetary disk are connected to its parent molecular cloud. This configuration is naturally expected if we consider disk formation by the gravitational collapse of the cloud core. Observations of some

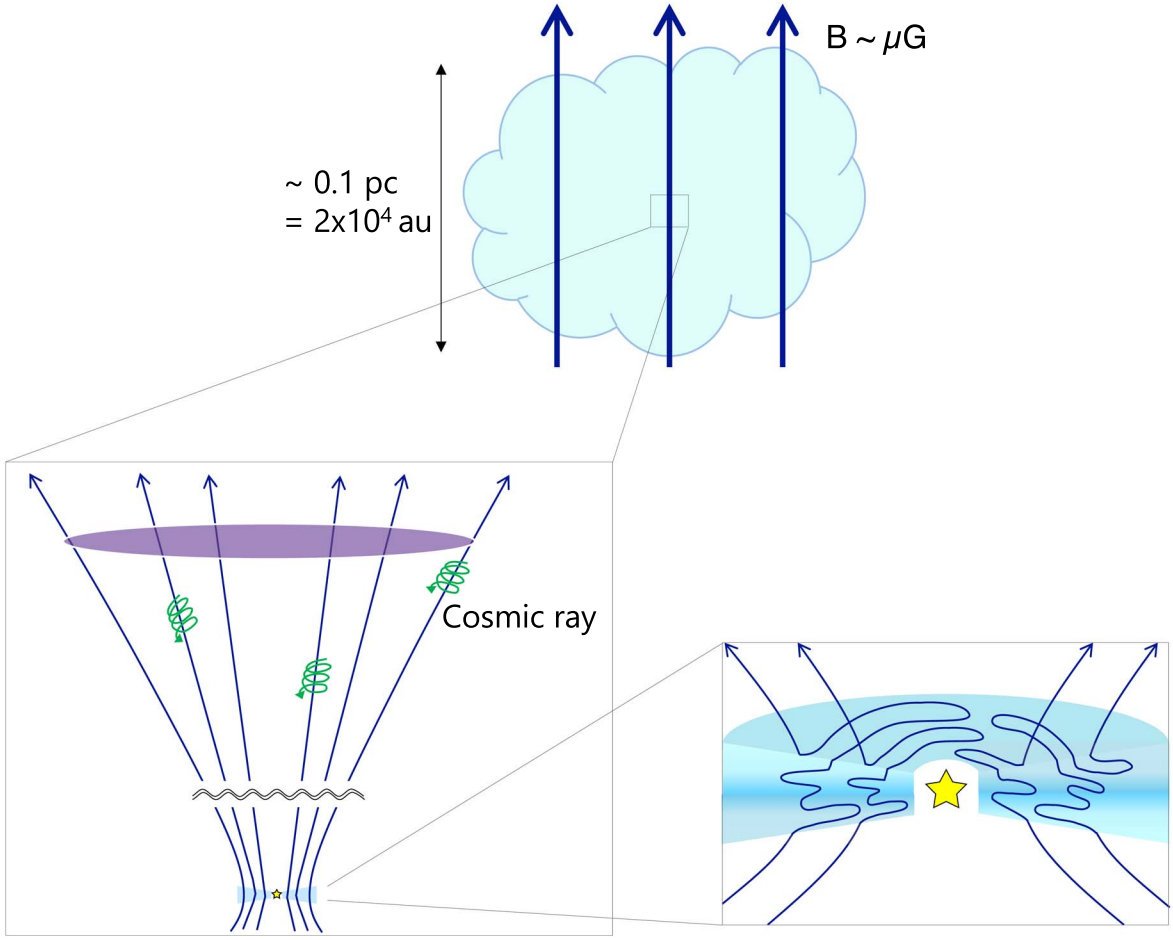

Figure 1. Schematic view of our scenario. An hourglass-shaped magnetic-field configuration focuses cosmic rays from a molecular cloud core to a protoplanetary disk. The purple oval represents the area from which the disk can receive cosmic-ray particles. The magnetic fields are stretched to azimuthal direction by shearing motion.

molecular cloud cores show an hourglass-shaped magnetic-field configuration, which may support this picture (e.g., Maury et al. 2018). This configuration is similar to those used by Padovani & Galli (2011), Padovani et al. (2013). In contrast, the magnetic fields in the solar wind extend horizontally with a spiral shape and are disconnected from those in the ISM(Parker 1958; Peterson et al. 2019). If the magnetic-field configuration around a protoplanetary disk is similar to that of the solar wind, the cosmic-ray density can be modulated due to T-Tauriosphere as discussed in Cleeves et al. (2013,2014, 2015). However, in the case that magnetic fields are connected to the ISM, cosmic rays can travel along the field lines (see Section 5).

The gyro radius of a cosmic-ray proton is $r_G = E/(eB) \sim 0.2(E/10\,\mathrm{GeV})(B/10\,\mu\mathrm{G})^{-1}$ au, where E is the energy of cosmic-ray protons, e is the elementary charge, B is the magnetic field strength, and we use $B = 10\,\mu$G in a molecular cloud (e.g., Crutcher et al. 2010). This is much smaller than the scale of the cloud core ($\sim$0.1 pc $\sim 2 \times 10^4$ au), which can be regarded as the turbulence scale.[5] Thus, cosmic rays of $E \lesssim 10$ TeV travel along magnetic-field lines. We assume that cosmic-ray propagation is in the free-streaming regime and ignore the diffusion (see Section 5). The disk bundles up the magnetic-field lines from a large area.[6] If we assume that the cosmic-ray flux is proportional to the magnetic field strength, which is true for an isotropic cosmic-ray distribution and inefficient cosmic-ray diffusion perpendicular to the magnetic-field lines, the cosmic-ray flux at the disk surface is enhanced by a factor of

$$\frac{S_{\mathrm{cloud}}}{S_{\mathrm{disk}}} = \frac{B_{\mathrm{disk}}}{B_{\mathrm{cloud}}} \sim 10^3, \tag{1}$$

where S_{cloud} is the surface area in the molecular cloud from which the protoplanetary disk can collect cosmic rays (the purple area in Figure 1), S_{disk} is the total area of the disk, and $B_{\mathrm{disk}} \sim 10$ mG and $B_{\mathrm{cloud}} \sim 10\mu$G are the typical strengths of magnetic fields in a protoplanetary disk (at $r \sim 10$ au, $z \sim 4H$, where H is the scale height of the disk; cf., Suzuki et al. 2010) and molecular cloud core, respectively.

In accordance with the conservation of kinetic energy and magnetic moment of a cosmic-ray particle, the pitch angles of the particles in a molecular cloud core, α_{cloud}, and that in a protoplanetary disk, α_{disk}, have the following relation (e.g.,

[5] We consider that the kinetic-scale turbulence can be damped due to the low ionization rate in the cloud core and the disk. Also, the turbulence should be injected in the largest scale, and the power spectrum of MHD turbulence is expected to be steep (Goldreich & Sridhar 1995).

[6] During the star and disk formation, a part of the magnetic fields slips out from the disk. We use the magnetic field strength after the disk formation in our estimate.

Padovani & Galli 2011):

$$\frac{\sin^2\alpha_{\rm disk}}{\sin^2\alpha_{\rm cloud}}=\frac{B_{\rm disk}}{B_{\rm cloud}}. \quad (2)$$

If we adopt the value in Equation (1), the pitch angle in the cloud core should satisfy $\sin\alpha_{\rm cloud}\leqslant 0.03$, which means that only the cosmic-ray particles that travel almost perfectly parallel to the field line can enter the protoplanetary disk. All the other particles are reflected by the magnetic mirror effect, and the cosmic-ray flux is reduced by a factor of $\alpha^2/2$. Because of the balance between the focusing and reflecting effects, the net cosmic-ray flux at the disk surface ends up being half of that in the parental cloud core (see Silsbee et al. 2018, for more detailed treatment). This factor 2 is generic as long as $B_{\rm cloud}/B_{\rm disk}\ll 1$. We define this factor for diminishing cosmic-ray flux as $\Gamma_{\rm dim}$.

3. Disk Structure

Below the disk surface, the magnetic fields are stretched to the azimuthal direction due to the shear motion of the disk (see Figure 1). In order to obtain the sheared field structure and the stratified density distribution of a protoplanetary disk, we perform MHD simulations. The circumstance under which magnetorotational instability (MRI) generates turbulence is still controversial (Bai & Stone 2013; Bai 2013; Gressel et al. 2015; Simon et al. 2015; Mori et al. 2019). The activation of MRI is strongly affected by the ionization-rate distribution, which will be obtained in this work. In this Letter, we consider a nonturbulent protoplanetary disk because it leads to the most efficient ionization by cosmic rays (see Section 5 for the effect of turbulence). We conduct low-resolution shearing-box simulations with ideal MHD approximation (Goldreich & Lynden-Bell 1965; Hawley et al. 1995) to mimic the nonturbulent disk structure.

The simulations were performed with Athena MHD code (Stone et al. 2008; Stone & Gardiner 2010). The benefit of the ideal MHD approximation is that simulations can be done with normalized physical values (Keplerian frequency, scale height of the disk, and the midplane density are set to be unity). We can freely scale the unit to arbitrary radii in the disk. The resolution was $30\times 60\times 240$ for a local box with the size of $\pm 0.5\,H$, $\pm 1\,H$, and $\pm 4\,H$ in the x, y, and z directions, respectively. The z-component of the initial plasma beta in the midplane of the disk (corresponding to the net vertical field) is parameterized as $\beta_z=10^4$ and 10^6.

The top panel of Figure 2 shows the ratio of the y and z components of the magnetic fields as a function of the distance from the midplane for $\beta_z=10^6$. One can see that the shear elongates the field lines to the azimuthal direction by a factor of 100−1000. This means that the cosmic-ray particles traveling along the magnetic fields have to go through $\Gamma_{\rm detour}=\int\langle B_y/B_z\rangle dz\sim$ 100–1000 times longer distance to arrive at a certain height than the vertically straight path. Although the absolute values of the field strength are different between the cases with $\beta_z=10^4$ and 10^6, the values of $\Gamma_{\rm detour}$ are similar. Thus, our results can be applied to the disks that have typical magnetic fields ($\beta_z=10^4$–10^6). We cautiously note that the averaging procedure will affect the detouring factor; $\langle B_y/B_z\rangle$ is different from $\langle B_y\rangle/\langle B_z\rangle$. When we compute the values in the brackets, we first horizontally average the data and take a time average for 50 orbital periods from the point of 350 orbits after the beginning of the simulation.

Taking the effect of detouring into consideration, we estimate the effective column density that cosmic rays have to go through to enter into the disk. The results are presented in the bottom panel of Figure 2 for the disk around IM Lup (Zhang et al. 2021) as an example of the observed protoplanetary disks. With conventional treatment, the cosmic rays of an attenuation length of $\sim$100 g cm^{-2} (Umebayashi & Nakano 1981; see Padovani et al. 2018 for more updated values for the high-density region) can arrive at the midplane for $r\gtrsim 10$ au unless the shielding effect by T-Tauriosphere is effective. On the other hand, our treatment indicates that cosmic rays cannot arrive at the disk midplane even at $\sim$100 au for IM Lup.

In our simulations, the toroidal component of magnetic fields is generated at all heights due to the ideal MHD approximation. In the very dense region with poor coupling with magnetic fields, i.e., near the midplane around a few astronomical unit from the star, the field lines would not be stretched by the velocity shear. Then, cosmic rays do not have to detour much. In such a region, however, cosmic rays are easily shielded, and our conclusions are unchanged.

4. Effects on the Ionization Rates

We show a significant enhancement of the effective column density in Figure 2. Due to the detouring of the cosmic rays along the sheared field lines, the cosmic-ray particles stay in the surface layer for a longer time before they enter into the disk. The cosmic-ray ionization rate at the point of interest within the disk can be calculated as

$$\zeta_{\rm CR}=\frac{1}{2}\Gamma_{\rm dim}\,\zeta_{\rm ISM}\{\exp(-\Gamma_{\rm detour}\chi_{\rm eff,u}/\chi_{\rm CR}) + \exp(-\Gamma_{\rm detour}\chi_{\rm eff,l}/\chi_{\rm CR})\}, \quad (3)$$

where $\zeta_{\rm ISM}$ is the ionization rate of cosmic rays in the ISM, and $\chi_{\rm CR}=96$ g cm^{-2} is the attenuation length of cosmic rays (Umebayashi & Nakano 1981). We define the vertical column density from the point to the upper and lower surface of the disk as $\chi_{\rm eff,u}$ and $\chi_{\rm eff,l}$, respectively, and $\Gamma_{\rm detour}$ is the ratio of the effective and vertical column density from the point to the closer surface, i.e., $\Gamma_{\rm detour}=1$ in conventional studies, and $\Gamma_{\rm detour}\chi_{\rm eff}=\int\langle\rho B_y/B_z\rangle dz$ in our work. Our results suggest $\Gamma_{\rm detour}\sim 100$ when the cosmic rays travel along the sheared magnetic fields. Intuitively, one would think that the cosmic-ray density can be enhanced by the sheared magnetic field by a factor of $\Gamma_{\rm detour}$. However, the sheared magnetic field makes the mirroring effect effective, and thus, the cosmic-ray density does not change (see Section 2).

As an example, we estimate the ionization rate assuming the surface density and temperature distributions of the disk around IM Lup (Zhang et al. 2021). We consider 4 ionization sources: cosmic rays, X-rays, short-lived radionuclides (SLR), and long-lived radionuclides (LLR). The cosmic-ray ionization rate is given by Equation (3). The typical value used in conventional studies is $\zeta_{\rm ISM}=10^{-17}$ s^{-1} (Spitzer & Tomasko 1968; Cummings et al. 2016), and we adopt this for the conventional model. Observations of diffuse clouds in the Galactic disk suggest higher values (Padovani et al. 2020); however, those values are not consistent with a lower ionization rate in the

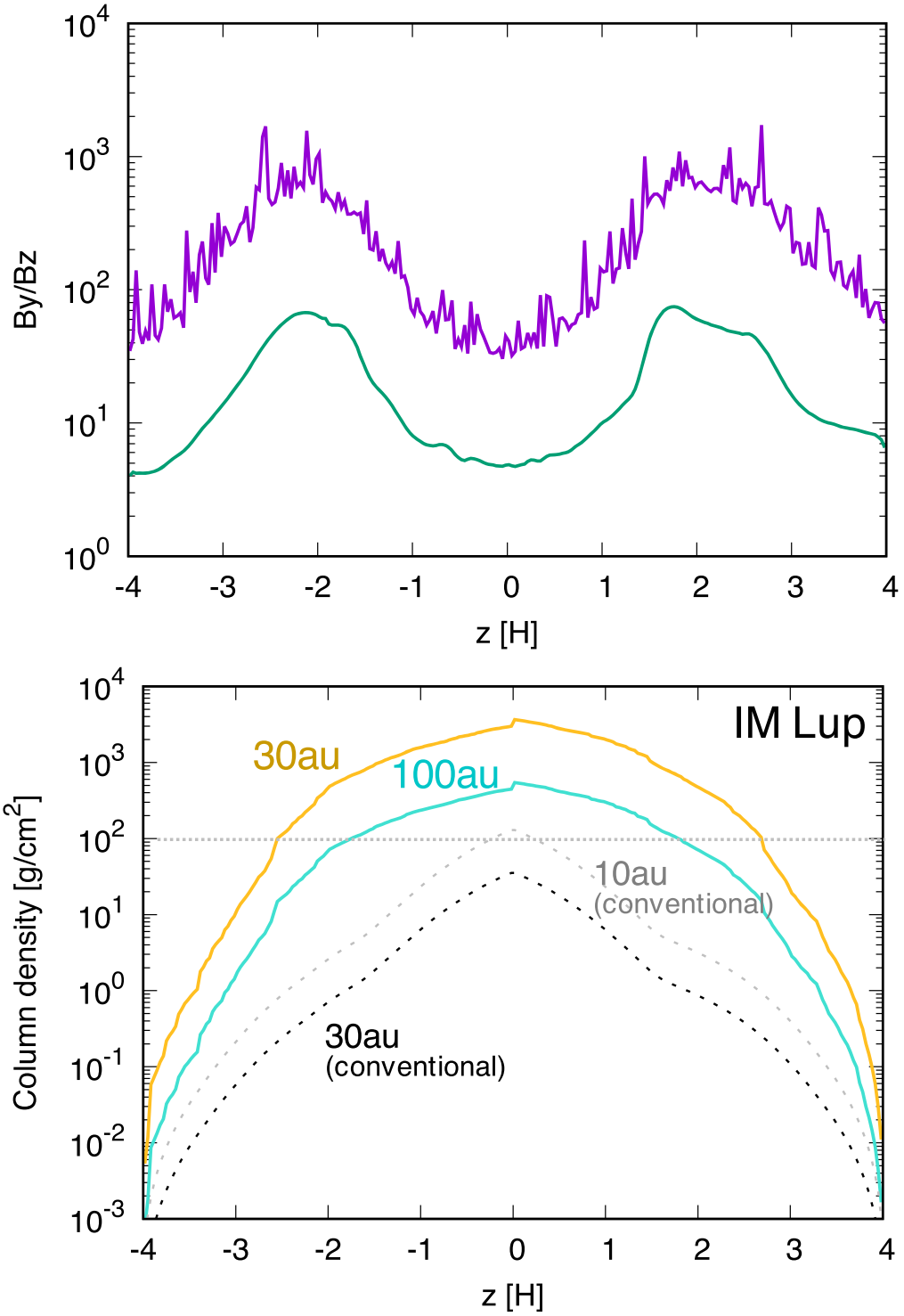

Figure 2. The top panel shows the ratio of the azimuthal and vertical components of the magnetic field strength at each height from the midplane. The purple jagged line represents $\langle B_y/B_z\rangle$. We also plot $\langle B_y\rangle/\langle B_z\rangle$ in green for comparison. The bottom panel presents the effective column densities that cosmic-ray particles have to go through from the closer surface to reach the corresponding heights. The dashed curves are the vertical column densities that are used in the conventional estimates, and the dotted horizontal line represents the attenuation length of cosmic rays.

midplane of protoplanetary disks (Aikawa et al. 2021; Seifert et al. 2021). Here, we employ $\zeta_{\rm ISM} = 3\times10^{-16}$ s^{-1} (Indriolo et al. 2015) for our new estimates. The value of $\Gamma_{\rm detour}$ is insensitive to the averaging method; the calculations of $\langle\rho\, B_y/B_z\rangle$ and $\langle\rho\rangle\langle B_y/B_z\rangle$ lead to similar results. We use the X-ray ionization rate by Bai (2011) that considers both the direct and scattered emissions based on Igea & Glassgold (1999). We use X-ray luminosity $L_X = 10^{30}$ erg s^{-1} (Cleeves et al. 2017) and plasma temperature $T_X = 3$ keV. The ionization rate by SLR and LLR are $\zeta_{\rm SLR} = 7.6\times10^{-19}$ s^{-1} and $\zeta_{\rm LLR} = 1.4\times10^{-22}$ s^{-1}, respectively (Umebayashi & Nakano 2009).

The top panel of Figure 3 shows the ionization rates as a function of r at $z = 2H$. We can see that cosmic rays are attenuated above $z = 2H$, and the X-ray ionization is dominant

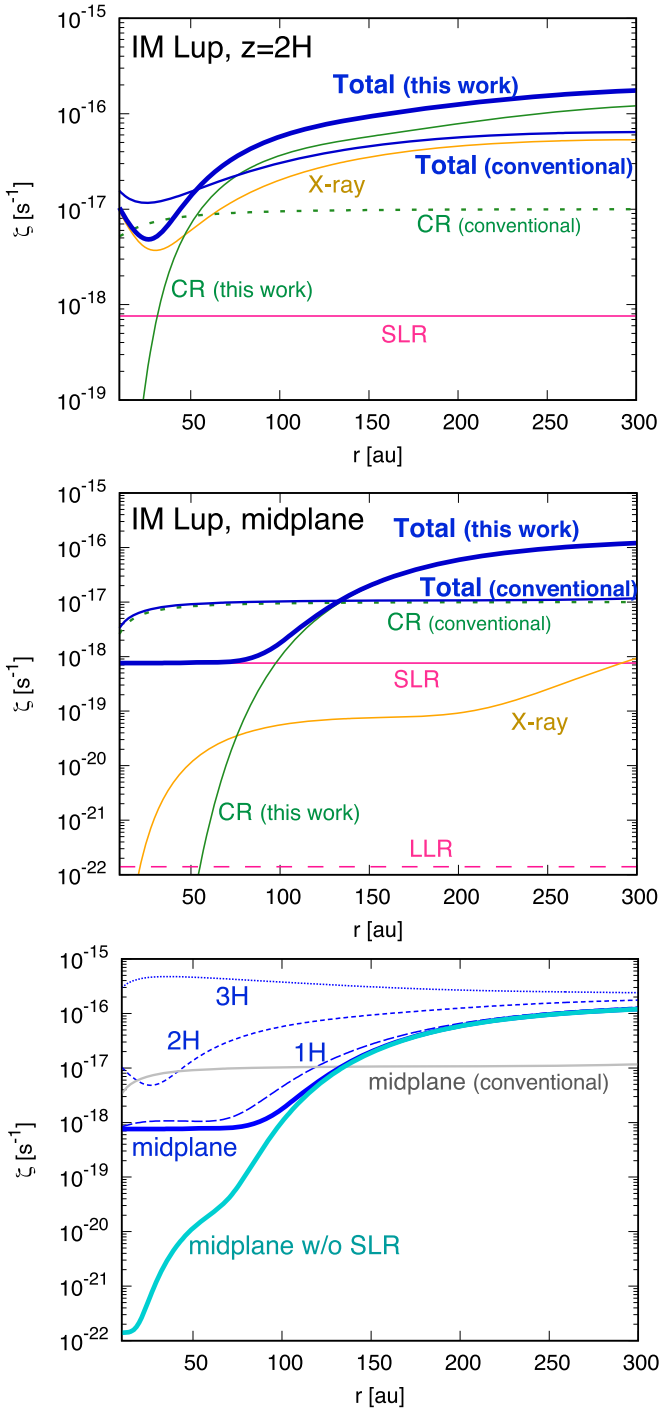

Figure 3. Top panel: the radial distribution of ionization rate, at $2H$ from the midplane based on the new estimate of the cosmic-ray ionization rate (solid green) with $\zeta_{\rm ISM} = 3 \times 10^{-16}$ s^{-1} using the effective column density along the elongated path, together with the contribution of X-ray (orange) and short-lived radionuclides (SLR; pink), is displayed with the thick blue curve. The conventional estimate of $\zeta_{\rm CR}$ based on $\zeta_{\rm ISM} = 10^{-17}$ s^{-1} with $\Gamma_{\rm detour} = 1$ (the dotted green line) makes up the thin blue curve of the conventional ionization rate. Middle panel: the same as with the top panel, but for the midplane of the disk. The dashed pink line is the ionization rate of the long-lived radionuclides (LLR). Bottom panel: the total ionization rate at $z = 3H$, $2H$, $1H$, and midplane using the cosmic-ray ionization rate of this work. The case with the absence of SLR and the estimate using the conventional cosmic-ray ionization rate are plotted in light blue and gray, respectively. The x-axis in each plot starts from 10 au.

for $r \lesssim 50$ au. On the other hand, the conventional treatment leads to the opposite trend: the X-ray ionization is dominant at outer radii, while cosmic-ray ionization is important in the inner part of the disk.

The modification of the ionization rate in the midplane is summarized in the middle panel of Figure 3. In the conventional model, cosmic rays are the dominant ionization source for all the radii. On the other hand, the cosmic-ray ionization rate of our model at $r \lesssim 100$ au is much lower than that of the conventional model because of the significant reduction of the cosmic-ray flux. The ionization is dominated by SLR there. The X-ray ionization is subdominant in all radii, because of the significant attenuation.

$\zeta_{\rm ISM}$ higher than the conventional model does not affect the total ionization rate in the upper layers of $z \gtrsim 3H$, because the X-ray ionization rate is higher at the upper layer of the disk. When the X-ray flux is much smaller, the ionization rate may be dominated by the adopted $\zeta_{\rm ISM}$ even in the higher atmosphere of the inner disk.

The half-life of the most effective species among SLR, ^{26}Al, is 7×10^5 years, and they might not necessarily still be present in the protoplanetary disks of interest (see Section 5 for the discussion on the production of ^{26}Al). Thus, we calculate the ionization rate of the disk in the absence of the SLR (the bottom panel of Figure 3). The ionization is actually led by LLR within $\sim$20 au in this case. Then, X-rays play an important role for 20 au $\lesssim r \lesssim$ 70 au, and cosmic rays are dominant for $r \gtrsim 70$ au. Umebayashi & Nakano (2009) pointed out that the ionization by radionuclides suddenly becomes inefficient when the mean size of the dust grains grows to about $>$1 cm because the radiation is absorbed by the grains. In such a case, ionization would be governed by X-rays while cosmic rays are highly attenuated.

The 2D map of the ionization rate for our new model and that for the conventional estimate are shown in Figure 4. The ionization rate for our model is lower than that for the conventional model by about an order of magnitude for $z \lesssim 1H$ and $r \lesssim 100$ au due to the detouring of cosmic rays. The ionization rate in this region is dominated by SLR in our model, while the cosmic-ray ionization is dominant in the conventional model (see the distribution of green dots in the figure). On the other hand, the ionization rate for our model is higher than that for the conventional model for $z \sim 2H$ or the midplane for $r \gtrsim 120$ au, owing to the larger value of $\zeta_{\rm ISM}$.

5. Discussion

The suppression of the energy density of cosmic rays with energies $<$10 GeV is observed in the solar system (Potgieter 2013). The situation in the protostellar system is more speculative. Some claim that winds from young stars should suppress the cosmic rays of similar or even higher energies (Cohen et al. 2012; Rodgers-Lee et al. 2020b). However, we consider that the T-Tauri winds are unlikely to affect the cosmic-ray density in the protoplanetary disks. The mass outflow rate from T-Tauri stars is much lower than the winds from protoplanetary disks, and then, the T-Tauri winds cannot push out the disk winds. Thus, the disk winds fill the region above the disk and may modulate the cosmic-ray density. We speculate that the magnetic-field configuration is crucial for the

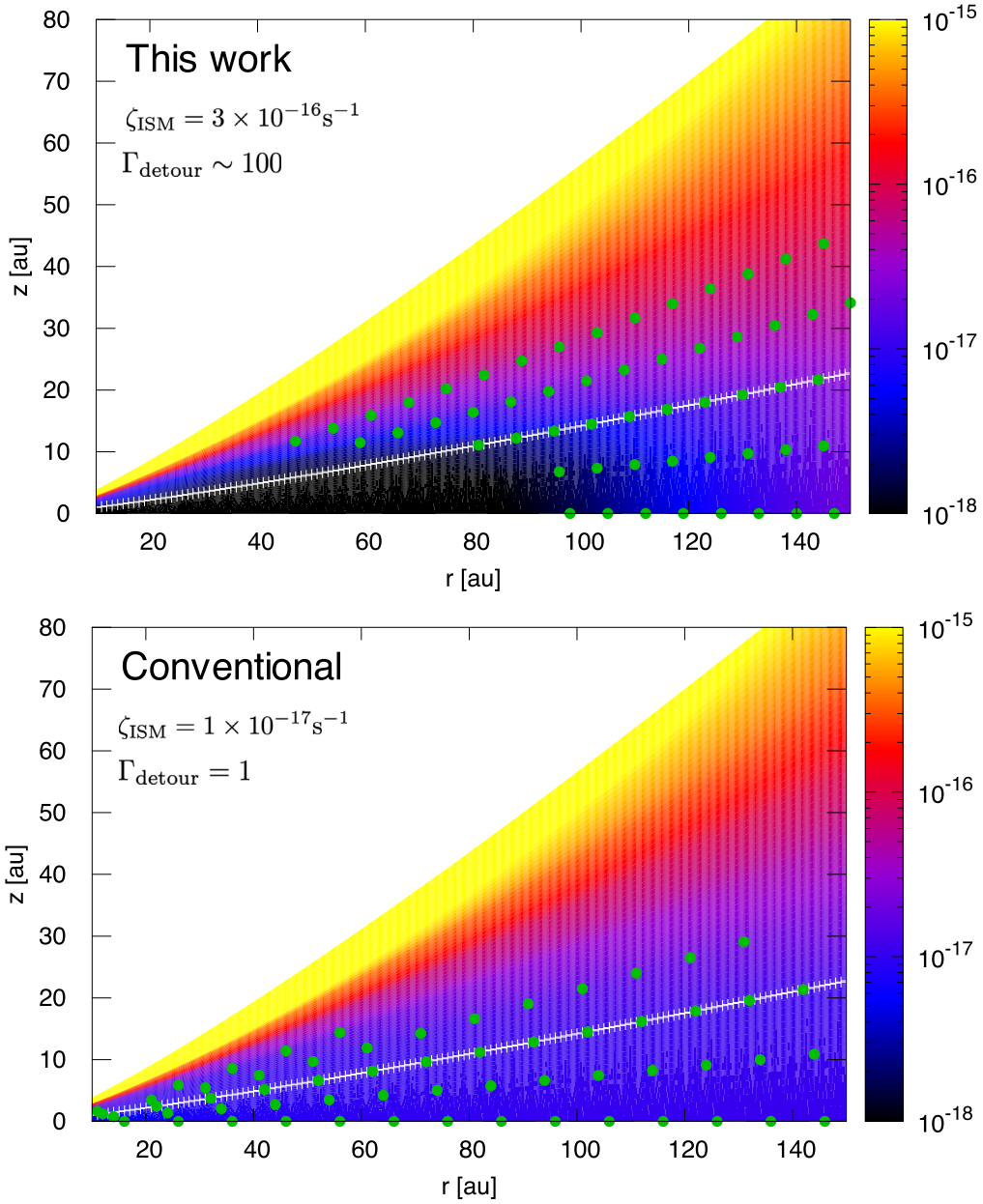

Figure 4. The distribution of ionization rate for our new model considering the propagation of cosmic rays along magnetic fields and that for the conventional model considering the vertical attenuation of cosmic rays in the disk around IM Lup. The white lines represent the scale height of the disk (which is $\sqrt{2}$ times larger than the definition of Zhang et al. 2021), and the green dots mark the regions where the cosmic rays are the dominant ionization source.

suppression of cosmic rays. If the disk winds are driven by the magnetic centrifugal force (Blandford & Payne 1982; Bai et al. 2016), the magnetic-field lines anchored in the disk can be connected to the ISM, and the magnetic-field lines are not completely dominated by the toroidal component. Then, the cosmic rays are likely able to enter the disk by the free-streaming or diffusion parallel to the magnetic field lines. On the other hand, if the disk winds are driven by other mechanisms, such as turbulence heating (Suzuki et al. 2010) or photoevaporation (Owen et al. 2010; Kimura et al. 2016a; Kunitomo et al. 2020, 2021), the magnetic-field lines are unlikely connected to the ISM and likely dominated by the toroidal component. Then, the cosmic rays need to cross the magnetic-field lines many times to reach the disk, which may suppress low-energy cosmic rays as in the solar winds.

Stellar energetic particles are regarded as a possible ionization source in protoplanetary disks. Depending on the settings of calculations, such as the particle energy and the treatment of propagation, they may be the dominant or important ionization source in the surface layer of the disk (Turner & Drake 2009; Rab et al. 2017; Fraschetti et al. 2018) or even at the midplane of the disk (Rodgers-Lee et al. 2020a). However, even for high-energy particles of $E \sim 10\,{\rm GeV}$, the Larmor radius is much smaller than the scale height, and they need to detour along the sheared magnetic fields as long as the diffusion perpendicular to the magnetic-field lines are inefficient. Based on our scenario, stellar energetic particles may significantly contribute to the ionization rate at the disk surface, but they are unlikely to reach the midplane of the disk. Recent studies suggest ^{26}Al

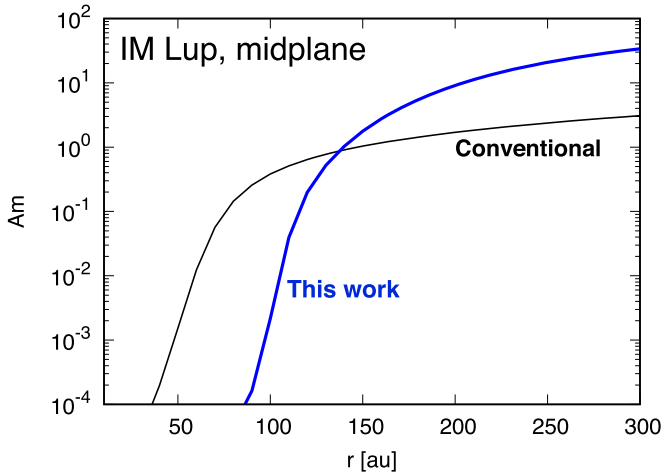

Figure 5. Radial distributions of ambipolar Elsässer number at the midplane of the disk around IM Lup.

can be produced by stellar energetic particles (Gaches et al. 2020; Adams 2021). However, since the stellar energetic particles cannot reach the disk midplane, the newly synthesized ^{26}Al is unlikely to affect the ionization rates in the range of our interest.

An ALMA large program, "Molecules with ALMA at Planet-forming Scales" discussed the ionization rates at the midplane of protoplanetary disks (Aikawa et al. 2021). Their results suggest $\zeta \sim 10^{-18}\,\mathrm{s}^{-1}$ and also show the variation among disks of a similar mass range. This might be caused by the different configurations of magnetic-field lines or the turbulent state of the disks. Another ALMA observation by Seifert et al. (2021) reported a lower ionization rate in the inner disk and a higher value in the outer radii with the transition at ∼80–100 au in the disk around IM Lup. Our model predicts a similar tendency as seen in Figure 4.

Some protoplanetary disks show lower values of the CO abundance compared to the canonical ISM value of 10^{-4} in the layer between the CO photodissociation layer in the surface and the CO freeze-out layer near the midplane (e.g., Favre et al. 2013; Miotello et al. 2017). This may suggest a high ionization rate of $\zeta \geqslant 10^{-17}\,\mathrm{s}^{-1}$ and low temperature ($T \sim 20$–30 K) in the disks because CO molecules are converted into less volatile molecules in such an environment (Furuya & Aikawa 2014; Bosman et al. 2018; Schwarz et al. 2018). Our model with the large value of $\zeta_{\rm ISM}$ predicts higher ionization rates at the middle layer ($\sim 2\,H$) in the outer disks (∼100 au) compared to the canonical cosmic-ray ionization rate, while keeping the midplane ionization rate as low as the values suggested by ALMA observations.

Bai & Stone (2013), Bai (2013), Simon et al. (2015) showed that ambipolar diffusion weakens the MRI turbulence at the outer radii of disks. We calculate the ambipolar Elsässer number $\mathrm{Am} = v_A^2/(\eta_A \Omega)$, where v_A, η_A, Ω are Alfvén velocity, ambipolar diffusivity, and Keplerian frequency, respectively. We use the formulae of Wardle (2007) for η_A and compute the ionization rate with the simplified method of Fujii et al. (2011). Figure 5 shows Am in the IM Lup disk. Our ionization model suggests $\mathrm{Am} \lesssim 1$, where we expect a purely laminar disk, within ∼150 au. The tendency that the disk is laminar at ∼100 au is consistent with the recent ALMA observation suggesting very weak turbulence due to the small scale height of the dust disk in the disk around Oph 163131 (e.g., Villenave et al. 2022). In the farther outer disk, where previous studies predict weak MRI turbulence due to ambipolar diffusion (Bai & Stone 2013; Bai 2013; Simon et al. 2015), our model expects $\mathrm{Am} \gtrsim 10$. This may fully activate the MRI turbulence. Depending on the location, the Hall effect might be the dominant nonideal MHD effect (Wardle & Salmeron 2012). Nonideal MHD simulations with our ionization model are required to further investigate the level of turbulence.

The existence of turbulence affects cosmic-ray transport. We have assumed that the magnetic fields have no fluctuations, and cosmic-ray transport is in the free-streaming regime. If some mechanism, such as MRI, drives turbulence, the fluctuations of magnetic fields can scatter the cosmic rays. Then, the cosmic-ray transport should be in the diffusion regime. Even in the diffusion regime, cosmic rays move along the magnetic-field lines because they have an anisotropic diffusion coefficient with the parallel diffusion much faster than the perpendicular diffusion, as shown in particle simulations in MRI turbulence (Kimura et al. 2016b, 2019; Sun & Bai 2021). Then, the particle trajectory can be expressed by the random walk along the field line. Thus, the path length to the disk midplane in the diffusion regime should be much longer than that in the streaming regime. In the diffusion regime, cosmic rays likely lose their energy at a farther upper region of the disk, and then, the ionization degree around the midplane of the disk would become low. This leads to suppression of turbulence, and cosmic rays would become able to enter the disk again. In summary, we start the discussion from the laminar magnetic field (implying suppression of turbulence). Then, cosmic rays will enhance the ionization rate, and the disk will become the ideal MHD regime that drives turbulence. The turbulence would shield the cosmic rays, which leads to the nonideal MHD regime in which turbulence is suppressed. To consistently understand the evolution of protoplanetary disks, we need to solve the MHD, cosmic-ray transport, and ionization rate simultaneously.

6. Summary

We have investigated the effects of the magnetic-field configurations on cosmic-ray ionization rates in protoplanetary disks. We have first considered the cosmic-ray propagation from ISM to the disk, where magnetic field strength changes by several orders of magnitude (see Figure 1). The cosmic-ray density at the disk surface should decrease by a factor of $\Gamma_{\rm dim} \sim 1/2$ from the ISM value because of the balance between the magnetic-flux focusing and reflection by a magnetic mirror.

The magnetic fields are stretched to the azimuthal direction in the disk due to the shearing motion, which affects the cosmic-ray distributions in the protoplanetary disks. Cosmic rays need to detour to reach the disk midplane due to the shearing magnetic field, and the vertical penetration depth should decrease. We have performed a set of local MHD simulations to obtain the detouring path length and showed that the cosmic-ray density at midplane for $r \lesssim 100$ au can be significantly suppressed even when we employ $\zeta_{\rm ISM} = 3 \times 10^{-16}\,\mathrm{s}^{-1}$. Our results suggest a totally different ionization rate distribution from that of the conventional model. This may change the chemical and dynamical evolution of the

protoplanetary disks, which is crucial to understanding the star and planet formation processes.

We acknowledge Satoshi Okuzumi, Yusuke Tsukamoto, Jiro Shimoda, Yuri Aikawa, Kenji Furuya, Yoshihide Yamato, and Akimasa Kataoka for useful discussions. We are grateful to Soonyoung Roh and Marco Padovani for fruitful discussions at the beginning of this project. We also thank Kedron Silsbee and Alexei Ivlev for useful comments. This work is partly supported by JSPS KAKENHI grant No. 19H05077, 22K14086 (Y.I.F), 19J00198, 21H04487, and 22K14028 (S. S.K.). Y.I.F was supported in part by the Program for the Development of Next-generation Leading Scientists with Global Insight (L-INSIGHT), sponsored by the Ministry of Education, Culture, Sports, Science and Technology (MXT), Japan. S.S.K. acknowledges the support by the Tohoku Initiative for Fostering Global Researchers for Interdisciplinary Sciences (TI-FRIS) of MEXT's Strategic Professional Development Program for Young Researchers. Numerical computations were in part carried out on Cray XC50 at Center for Computational Astrophysics, National Astronomical Observatory of Japan.

Appendix
Minimum Mass Solar Nebula Model

For the comparison with theoretical studies adopting the minimum mass solar nebula (MMSN) model (Hayashi 1981), we provide the effective column density for cosmic rays to arrive at various heights from the midplane of MMSN. Conventionally, cosmic rays are thought to easily reach the midplane at ∼10 au. As one can see in Figure 6, however, they can barely penetrate into the midplane at 100 au in our new model.

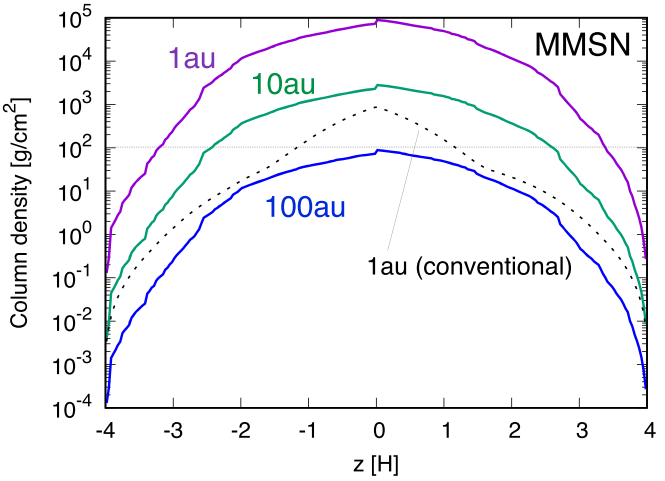

Figure 6. The effective column densities that cosmic rays have to pass through from the closer surface to reach each height of the MMSN at 1, 10, and 100 au. The dashed black line is the vertically measured column density that is used in conventional studies for 1 au. The thin horizontal line shows the attenuation length of cosmic rays.

ORCID iDs

Yuri I. Fujii https://orcid.org/0000-0002-3648-0507
Shigeo S. Kimura https://orcid.org/0000-0003-2579-7266

References

Adams, F. C. 2021, ApJ, 919, 10
Aikawa, Y., Cataldi, G., Yamato, Y., et al. 2021, ApJS, 257, 13
Bai, X.-N. 2011, ApJ, 739, 50
Bai, X.-N. 2013, ApJ, 772, 96
Bai, X.-N. 2017, ApJ, 845, 75
Bai, X.-N., & Stone, J. M. 2013, ApJ, 769, 76
Bai, X.-N., Ye, J., Goodman, J., & Yuan, F. 2016, ApJ, 818, 152
Béthune, W., Lesur, G., Ferreira, J., et al. 2017, A&A, 600, A75
Blandford, R. D., & Payne, D. G. 1982, MNRAS, 199, 883
Bosman, A. D., Walsh, C., & van Dishoeck, E. F. 2018, A&A, 618, A182
Cleeves, L. I., Adams, F. C., & Bergin, E. A. 2013, ApJ, 772, 5
Cleeves, L. I., Bergin, E. A., & Adams, F. C. 2014, ApJ, 794, 123
Cleeves, L. I., Bergin, E. A., Öberg, K. I., et al. 2017, ApJL, 843, L3
Cleeves, L. I., Bergin, E. A., Qi, C., Adams, F. C., & Öberg, K. I. 2015, ApJ, 799, 204
Cohen, O., Drake, J. J., & Kóta, J. 2012, ApJ, 760, 85
Crutcher, R. M., Wandelt, B., Heiles, C., Falgarone, E., & Troland, T. H. 2010, ApJ, 725, 466
Cummings, A. C., Stone, E. C., Heikkila, B. C., et al. 2016, ApJ, 831, 18
Eistrup, C., Walsh, C., & van Dishoeck, E. F. 2016, A&A, 595, A83
Ercolano, B., & Glassgold, A. E. 2013, MNRAS, 436, 3446
Favre, C., Cleeves, L. I., Bergin, E. A., Qi, C., & Blake, G. A. 2013, ApJL, 776, L38
Fraschetti, F., Drake, J. J., Cohen, O., & Garraffo, C. 2018, ApJ, 853, 112
Fromang, S., Terquem, C., & Balbus, S. A. 2002, MNRAS, 329, 18
Fujii, Y. I., Okuzumi, S., & Inutsuka, S. 2011, ApJ, 743, 53
Furuya, K., & Aikawa, Y. 2014, ApJ, 790, 97
Furuya, K., Aikawa, Y., Nomura, H., Hersant, F., & Wakelam, V. 2013, ApJ, 779, 11
Gaches, B. A. L., Walch, S., Offner, S. S. R., & Münker, C. 2020, ApJ, 898, 79
Gammie, C. F. 1996, ApJ, 457, 355
Glassgold, A. E., Najita, J., & Igea, J. 1997, ApJ, 480, 344
Goldreich, P., & Lynden-Bell, D. 1965, MNRAS, 130, 125
Goldreich, P., & Sridhar, S. 1995, ApJ, 438, 763
Gressel, O., Nelson, R. P., & Turner, N. J. 2012, MNRAS, 422, 1140
Gressel, O., Turner, N. J., Nelson, R. P., & McNally, C. P. 2015, ApJ, 801, 84
Hawley, J. F., Gammie, C. F., & Balbus, S. A. 1995, ApJ, 440, 742
Hayashi, C. 1981, PThPS, 70, 35
Igea, J., & Glassgold, A. E. 1999, ApJ, 518, 848
Ilgner, M., & Nelson, R. P. 2006, A&A, 445, 205
Indriolo, N., Neufeld, D. A., Gerin, M., et al. 2015, ApJ, 800, 40
Kimura, S. S., Kunitomo, M., & Takahashi, S. Z. 2016a, MNRAS, 461, 2257
Kimura, S. S., Toma, K., Suzuki, T. K., & Inutsuka, S.-i. 2016b, ApJ, 822, 88
Kimura, S. S., Tomida, K., & Murase, K. 2019, MNRAS, 485, 163
Kunitomo, M., Ida, S., Takeuchi, T., et al. 2021, ApJ, 909, 109
Kunitomo, M., Suzuki, T. K., & Inutsuka, S.-i. 2020, MNRAS, 492, 3849
Law, C. J., Loomis, R. A., Teague, R., et al. 2021, ApJS, 257, 3
Maury, A. J., Girart, J. M., Zhang, Q., et al. 2018, MNRAS, 477, 2760
Miotello, A., van Dishoeck, E. F., Williams, J. P., et al. 2017, A&A, 599, A113
Mori, S., Bai, X.-N., & Okuzumi, S. 2019, ApJ, 872, 98
Notsu, S., van Dishoeck, E. F., Walsh, C., Bosman, A. D., & Nomura, H. 2021, A&A, 650, A180
Öberg, K. I., Guzmán, V. V., Walsh, C., et al. 2021, ApJS, 257, 1
Okuzumi, S. 2009, ApJ, 698, 1122
Owen, J. E., Ercolano, B., Clarke, C. J., & Alexander, R. D. 2010, MNRAS, 401, 1415
Padovani, M., & Galli, D. 2011, A&A, 530, A109
Padovani, M., Hennebelle, P., & Galli, D. 2013, A&A, 560, A114
Padovani, M., Hennebelle, P., Marcowith, A., & Ferrière, K. 2015, A&A, 582, L13
Padovani, M., Ivlev, A. V., Galli, D., & Caselli, P. 2018, A&A, 614, A111
Padovani, M., Ivlev, A. V., Galli, D., et al. 2020, SSRv, 216, 29

Padovani, M., Marcowith, A., Hennebelle, P., & Ferrière, K. 2016, A&A, 590, A8
Parker, E. N. 1958, ApJ, 128, 664
Peterson, E. E., Endrizzi, D. A., Beidler, M., et al. 2019, NatPh, 15, 1095
Potgieter, M. S. 2013, LRSP, 10, 3
Rab, C., Güdel, M., Padovani, M., et al. 2017, A&A, 603, A96
Rodgers-Lee, D., Taylor, A. M., Downes, T. P., & Ray, T. P. 2020a, MNRAS, 491, 4742
Rodgers-Lee, D., Vidotto, A. A., Taylor, A. M., Rimmer, P. B., & Downes, T. P. 2020b, MNRAS, 499, 2124
Sano, T., Miyama, S. M., Umebayashi, T., & Nakano, T. 2000, ApJ, 543, 486
Schwarz, K. R., Bergin, E. A., Cleeves, L. I., et al. 2018, ApJ, 856, 85
Seifert, R. A., Cleeves, L. I., Adams, F. C., & Li, Z.-Y. 2021, ApJ, 912, 136
Silsbee, K., Ivlev, A. V., Padovani, M., & Caselli, P. 2018, ApJ, 863, 188
Simon, J. B., Lesur, G., Kunz, M. W., & Armitage, P. J. 2015, MNRAS, 454, 1117
Spitzer, L. J., & Tomasko, M. G. 1968, ApJ, 152, 971
Stone, J. M., & Gardiner, T. A. 2010, ApJS, 189, 142
Stone, J. M., Gardiner, T. A., Teuben, P., Hawley, J. F., & Simon, J. B. 2008, ApJS, 178, 137
Sun, X., & Bai, X.-N. 2021, MNRAS, 506, 1128
Suzuki, T. K., Muto, T., & Inutsuka, S.-i. 2010, ApJ, 718, 1289
Turner, N. J., & Drake, J. F. 2009, ApJ, 703, 2152
Turner, N. J., & Sano, T. 2008, ApJL, 679, L131
Umebayashi, T., & Nakano, T. 1981, PASJ, 33, 617
Umebayashi, T., & Nakano, T. 2009, ApJ, 690, 69
Villenave, M., Stapelfeldt, K. R., Duchêne, G., et al. 2022, ApJ, 930, 11
Walsh, C., Nomura, H., Millar, T. J., & Aikawa, Y. 2012, ApJ, 747, 114
Wardle, M. 2007, Ap&SS, 311, 35
Wardle, M., & Salmeron, R. 2012, MNRAS, 422, 2737
Zhang, K., Booth, A. S., Law, C. J., et al. 2021, ApJS, 257, 5